JACS
JOURNAL OF THE AMERICAN CHEMICAL SOCIETY
Article
Cite This: J. Am. Chem. Soc. XXXX, XXX, XXX−XXX
pubs.acs.org/JACS

$U_2@I_h(7)$-C_{80}: Crystallographic Characterization of a Long-Sought Dimetallic Actinide Endohedral Fullerene

Xingxing Zhang,[†] Yaofeng Wang,[†] Roser Morales-Martínez,[§] Jun Zhong,[‡] Coen de Graaf,[§,#] Antonio Rodríguez-Fortea,[§] Josep M. Poblet,*[,§] Luis Echegoyen,*[,∥] Lai Feng,*[,⊥] and Ning Chen*[,†]

[†]Laboratory of Advanced Optoelectronic Materials, College of Chemistry, Chemical Engineering and Materials Science, Soochow University, Suzhou, Jiangsu 215123, PR China

[§]Departament de Química Física i Inorgànica, Universitat Rovira i Virgili, c/Marcel·lí Domingo 1, 43007 Tarragona, Spain

[∥]Department of Chemistry, University of Texas at El Paso, 500 West University Avenue, El Paso, Texas 79968, United States

[⊥]Soochow Institute for Energy and Materials InnovationS (SIEMIS), College of Physics, Optoelectronics and Energy & Collaborative, Soochow University, Suzhou, Jiangsu 215006, PR China

[‡]Jiangsu Key Laboratory for Carbon-Based Functional Materials and Devices, Institute of Functional Nano and Soft Materials (FUNSOM), Soochow University, Suzhou, Jiangsu 215123, PR China

[#]ICREA, Pg Lluis Companys 23, Barcelona 08010, Spain

Supporting Information

ABSTRACT: The nature of actinide−actinide bonds has attracted considerable attention for a long time, especially since recent theoretical studies suggest that triple and up to quintuple bonds should be possible, but little is known experimentally. Actinide−actinide bonds inside fullerene cages have also been proposed, but their existence has been debated intensively by theoreticians. Despite all the theoretical arguments, critical experimental data for a dimetallic actinide endohedral fullerene have never been obtained. Herein, we report the synthesis and isolation of a dimetallic actinide endohedral metallofullerene (EMF), $U_2@C_{80}$. This compound was fully characterized by mass spectrometry, single crystal X-ray crystallography, UV−vis−NIR spectroscopy, Raman spectroscopy, cyclic voltammetry, and X-ray absorption spectroscopy (XAS). The single crystal X-ray crystallographic analysis unambiguously assigned the molecular structure to $U_2@I_h(7)$-C_{80}. In particular, the crystallographic data revealed that the U−U distance is within the range of 3.46−3.79 Å, which is shorter than the 3.9 Å previously predicted for an elongated weak U−U bond inside the C_{80} cage. The XAS results reveal that the formal charge of the U atoms trapped inside the fullerene cage is +3, which agrees with the computational and crystallographic studies that assign a hexaanionic carbon cage, $(I_h\text{-}C_{80})^{6-}$. Theoretical studies confirm the presence of a U−U bonding interaction and suggest that the weak U−U bond in $U_2@I_h(7)$-C_{80} is strengthened upon reduction and weakened upon oxidation. The comprehensive characterization of $U_2@I_h(7)$-C_{80} and the overall agreement between the experimental data and theoretical investigations provide experimental proof and deeper understanding for actinide metal−metal bonding interactions inside a fullerene cage.

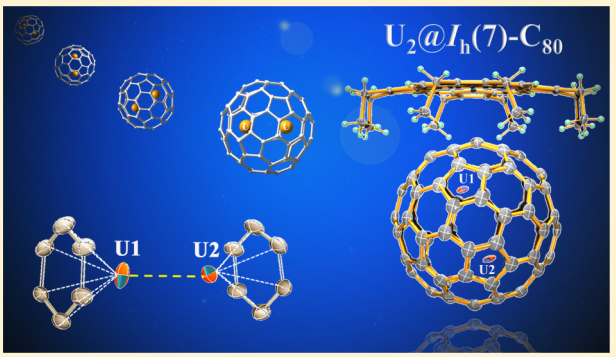

1. INTRODUCTION

Understanding chemical bonding is at the very heart of chemistry. The nature of actinide−actinide bonds has attracted considerable attention for a long time, especially since recent theoretical studies suggest that triple and up to quintuple bonds should be possible.[1−3] However, although metal−metal bonds for d-block elements have been intensively studied for transition metal compounds, not much is known experimentally for the chemical bond between actinide atoms.[4] To date, experimental evidence for diactinides are limited to mass spectroscopic observation of U_2 and Th_2 in the gas phase.[1] Although possible U−U interactions have been discussed for binuclear uranium compound, there is still no conclusive evidence of its existence and it remains as one of the holy grails of inorganic chemistry.[5] Difficulty with synthesis and characterization has largely hindered the exploration of actinide metal−metal bonds using conventional actinide chemistry. Matrix isolation methods were used to prepare $U(\mu\text{-}H_2)U$ and U_2H_4, characterized using infrared and DFT calculations, and these

Received: October 11, 2017
Published: January 27, 2018

DOI: 10.1021/jacs.7b10865
J. Am. Chem. Soc. XXXX, XXX, XXX−XXX

were described as "the first examples of an actinide−actinide bond".[6]

Endohedral metallofullerenes (EMFs) are known as ideal hosts for clusters that contain multiple metal ions.[7−9] It has been shown in numerous cases that clusters with unique electronic structures, which would not be stable independently, can be stabilized by charge transfer from the encapsulated ions or clusters to the cages.[10−12] Some of these encapsulated metal ions do not exhibit their highest oxidations states and result in covalent metal−metal bonds.[13,14] Lanthanide−lanthanide bonding inside fullerene cages has been intensively studied and the existence of La−La, Sc−Sc, Y−Y, and Tb−Tb single bonds have been experimentally established.[14−19] A very recent example is $Lu_2@C_{82}$, reported by Lu et al., in which two Lu ions in a +2 oxidation state form a Lu−Lu single bond.[20] Popov et al. also reported that in the benzyl monoadducts of $Dy_2@C_{80}$, a single-electron metal−metal bond was formed inside the C_{80} cage, resulting in remarkable single-molecule magnetism with a record high blocking temperature.[17]

Dimetallic uranium EMFs were originally experimentally observed by mass spectrometry by Smalley et al.[21] On the basis of their observations, it is reasonable to assume that actinide−actinide bonds, which are extremely difficult to prepare by conventional actinide chemistry, may be formed inside fullerene cages as stabilizing nanocontainers. This topic has been intensively debated by theoreticians in recent years. Lu et al. suggested that a 6-fold U−U bond could exist inside a C_{60} cage.[22] A subsequent report by Gagliardi et al. argued that this bond may be an artifact due to the small and constrictive size of the C_{60} cage.[23] They also predicted that inside larger cages, C_{70}−C_{84}, the two U atoms prefer to bond to the internal walls of the fullerene cages rather than forming a U−U bond. Very recently, theoretical studies by Straka et al. also predicted the existence of a cage-imposed U−U bond inside a C_{80} cage. Their study predicted a stable EMF, $U_2@I_h$-C_{80}, which has double ferromagnetic U−U bonds with a bond distance of 3.9 Å, although in the title of the article they call it "an unwilling U−U bonding".[24] Despite all the arguments from theoretical studies, critical experimental data for a dimetallic actinide EMF have never been obtained, leaving the possibility of forming actinide−actinide bonds inside fullerenes as an open question up to now. Herein, following the successful synthesis and characterization of $Th@C_{82}$[25] and $U@C_{82}$,[26] we present the synthesis, isolation, and full characterization of a dimetallic actinide EMF, $U_2@I_h(7)$-C_{80}. Critical crystallographic data were obtained in this study. These results reveal the crystal structure of $U_2@I_h(7)$-C_{80} and show that, though the U positions are disordered inside the fullerene cage, the U−U bond distance is within the range of 3.46−3.79 Å. The systematic characterization of $U_2@I_h(7)$-C_{80}, which agreed with theoretical studies, shows evidence of a weak U−U bonding interaction inside the C_{80} fullerene cage.

2. RESULTS AND DISCUSSION

$U_2@I_h(7)$-C_{80} was synthesized by a modified arc discharge method.[27] Graphite rods, packed with U_3O_8 and graphite powder, were vaporized in the arcing chamber under a He atmosphere.[26] The resulting soot was then extracted with chlorobenzene. The mass spectrum of an as-extracted solution of the fullerene mixture (Figure S1) shows that a large family of U based metallofullerenes with multiple cages was generated during the arcing process, along with empty fullerenes C_{2n} (n = 42−66). The mass spectrum shows that the majority of the fullerenes generated during this process are mono-EMF ($U@C_{2n}$) and empty fullerenes. $U_2@C_{80}$ was generated as a minor product during this process, along with the other dimetallic U based fullerenes $U_2@C_{78}$ and $U_2@C_{82}$. However, the previously reported and theoretically studied $U_2@C_{60}$ was not detected using these conditions. A multistage HPLC procedure was employed to isolate and purify $U_2@C_{80}$ (Figure S2). After a three-stage HPLC separation protocol, the purified $U_2@C_{80}$ was obtained. The purity of the isolated $U_2@C_{80}$ was confirmed as a single peak by HPLC (Figure 1b). The positive-ion mode

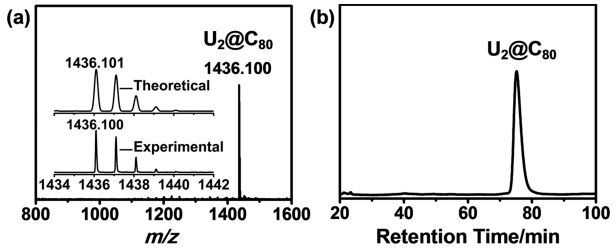

Figure 1. Positive-ion mode MALDI-TOF mass spectrum of purified $U_2@C_{80}$ (left). The inset shows the experimental and theoretical isotopic distribution for $U_2@C_{80}$. HPLC chromatogram of the $U_2@C_{80}$ (right); using a 10 mm × 250 mm Buckyprep column; flow rate 4.0 mL/min; toluene as moving phase.

MALDI-TOF mass spectrum of purified $U_2@C_{80}$ (Figure 1a) shows a peak at m/z = 1436.100, and the experimental isotopic distribution agrees well with the theoretical prediction.

The structure of $U_2@C_{80}$ was characterized by means of single crystal X-ray diffraction (XRD). The molecular structure was resolved and refined in the $C2/m$ space group. Figure 2

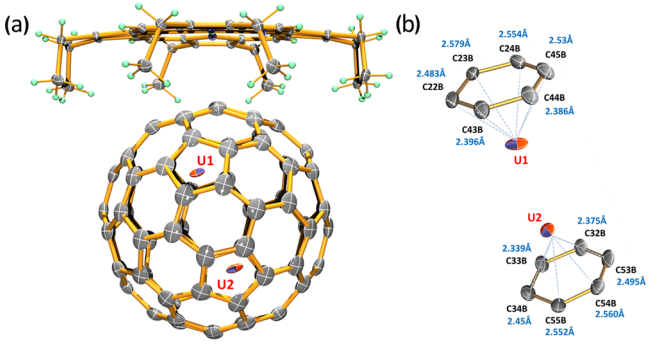

Figure 2. (a) Thermal ellipsoid drawing of $U_2@I_h$-C_{80}·[Ni^{II}(OEP)] with 20% thermal ellipsoids. Only the major U sites (U1 and U2 with a common occupancy of 0.195(2)) are shown. For clarity, the solvent molecules and minor metal sites are omitted. (b) View showing the interaction of the major U_2 cluster with the closest cage portion.

shows the X-ray structure of $U_2@I_h$-C_{80} together with a cocrystallized Ni^{II}-octaethyl porphyrin [Ni^{II}(OEP)] moiety. The typical host−guest interaction can be observed between the $U_2@C_{80}$ and the [Ni^{II}(OEP)] with the shortest Ni-to-cage carbon distance (Ni1−C23B) of 2.787(14) Å, very close to those reported for most EMF/[Ni^{II}(OEP)] complexes. For the fullerene moiety, an icosahedral symmetric $I_h(7)$-C_{80} cage (Figure 2) with two orientations that occupy a common site is clearly seen (see the Supporting Information for details on the crystallographic structures). The endohedral U_2 cluster is highly disordered. A total of 10 U sites can be identified, which can be classified into two groups (i.e., U1/U3/U5/U7/U9 and U2/

DOI: 10.1021/jacs.7b10865
J. Am. Chem. Soc. XXXX, XXX, XXX−XXX

U4/U6/U8/U10), each with the distribution over a belt-region near or opposite to the Ni^{II}(OEP) moiety (Figure 3). Among

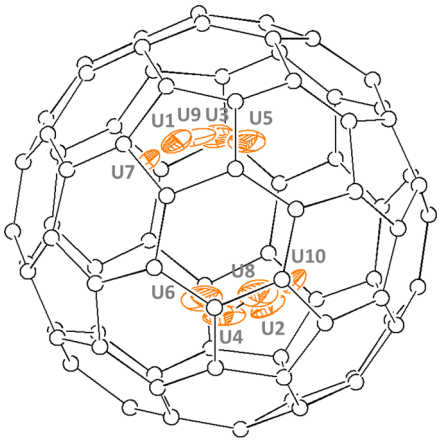

Figure 3. View showing the molecule in the same orientation as in Figure 2a and with all U positions (orange).

the multiple U sites, the U sites with similar occupancies were paired into sets during refinement, giving rise to five sets of U_2 with occupancies ranging from 0.195(2) to 0.0427(19). (See Figure 3 for disordered positions of U atoms). Only the U_2 cluster (i.e., U1 and U2) with major occupancy is shown in Figure 2. Nevertheless, because of the fact that crystallographic mirror plane mismatches the molecular symmetry and some of the U sites (i.e., U1−6, U8) are residing off the mirror plane, these U sites cannot be solely determined due to the presence of *C*2/*m* positional disorder (see Table S1). If only the major U sites (i.e., U1 and U2) are considered, then there are four X-ray models of the $I_h(7)$-C_{80} cage (i.e., S_i, S_{ii}, S_{iii} and S_{iv}, see Figure S3). In these models, metal positions are not very different from each other. In general, U1 and U2 are residing under hexagons, being close to or slightly off a C2 axis of the I_h-C_{80} cage. The U−U distance is found to be 3.723(6) Å in models S_i and S_{ii}, while the U−U distance is 3.751(6) Å for S_{iii} and S_{iv} models. Similarly, the U−U distance obtained from other U sites ranges from 3.793(7) to 3.46(2) Å (for details see Table S1). All these U−U distances are shorter than that reported for the U−U bond distance in the lowest energy minimum isomer $U_2@I_h(7)$-C_{80} calculated at the DFT/BP86/SVP/SDD computational level (3.894 Å).[24] As summarized in Table 1, compared

Table 1. Metal−Metal Distance [Å] of Dimetallic Endohedral Fullerenes with C_{80} Cage

compound	M−M distance [Å]	ref
$U_2@I_h(7)$-C_{80}	3.793−3.460	this work
$Ce_2@I_h$-C_{80}	3.833−3.767	28
$La_2@I_h$-C_{80}	3.840	29
$La_2@I_h$-$C_{80}(C_7H_7)$	3.779−3.676	19
$Dy_2@I_h$-$C_{80}(CH_2Ph)$	3.893/3.896	17

with the metal−metal bond distances reported for $Ce_2@I_h$-C_{80} and $La_2@I_h$-C_{80} (Ce−Ce: 3.767−3.833 Å and La−La: 3.840 Å), the U1−U2 distance is also slightly shorter.[28,29] Considering their similar ionic radii (1.01 Å for Ce^{3+}, 1.025 Å for U^{3+} and 1.032 Å for La^{3+}), the shorter U−U distance might indicate a stronger metal−metal bonding interaction. Moreover, as shown in Table 1, these U−U distances are even comparable to the recently reported La−La bond distance in $La_2@I_h$-$C_{80}(C_7H_7)$ and slightly shorter than the Dy−Dy distance in $Dy_2@I_h$-$C_{80}(CH_2Ph)$.[17,19] In the two above-mentioned cases, relatively strong single electron metal−metal bonds were recorded. Thus, the crystallographic data for the U−U distance, though somewhat uncertain because of the disordered U positions, show evidence that the two U atoms are weakly bonded inside the fullerene cage. Nevertheless, this U−U distance is evidently longer than twice the empirical single bond radius of uranium (2 × 1.7 Å = 3.4 Å),[30] suggesting that the U−U bond order is lower than one, which agrees with the previous theoretical prediction of an elongated weak bond. The closest U−C contacts are in a range of 2.377−2.578 Å (see Figure 3 and Table S1). Such U−C contacts agree well with the previously reported calculation results and are comparable to those found in the smallest EMF of $U@C_{28}^{2+}$, where the U-C closest contacts are within 2.44−2.51 Å.[31] In comparison, in models S_{ii}, S_{iii}, and S_{iv}, the closest U−C contacts are distributed over a wider range of 2.24−2.82, 2.24−2.69, and 2.264−2.82 Å, respectively (see Figure 3 and Tables S2−S5). Nevertheless, it is noteworthy that even the longest U−C distance (2.82 Å) is still very close to that reported for the U−$C_{methanide}$ bond (i.e., 2.779 Å),[32] indicating strong bonding-interactions between the U_2 cluster and the $I_h(7)$-C_{80} cage.

Purified $U_2@I_h(7)$-C_{80} shows a dark brown color in CS_2 solution. The UV−vis−NIR absorption spectrum of $U_2@C_{80}$ in CS_2 (Figure 4) is rather featureless except for two minor

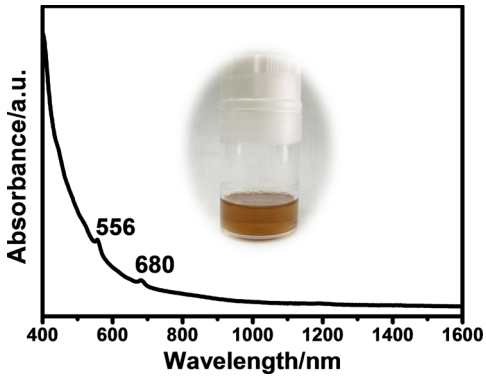

Figure 4. UV−vis−NIR absorption spectrum of $U_2@I_h(7)$-C_{80} in CS_2.

absorption peaks at 556 and 680 nm. Though featureless absorption spectra are typical for endohedral fullerenes with an I_h-C_{80} cage,[8] the absorption spectrum notably shows even less features than the representative I_h-C_{80} cage based endohedral fullerenes, such as $Sc_3N@I_h$-C_{80} and $La_2@I_h$-C_{80}. The absorption onset is ca. 1100 nm, which corresponds to a band gap of 1.13 eV.

The photoluminescence (PL) spectrum of the $U_2@I_h(7)$-C_{80} is shown in Figure 5. It shows broad emissions lines at 420, 450, and 476 nm. This emission pattern is similar to those typically observed for uranyl compounds, but the emission peaks are shifted substantially.[33] Very recently, we have reported that $Th@C_{3v}(8)$-C_{82} displays a strong PL emission in both solution and solid states, an unprecedented feature for fullerene compounds.[25] The observation of PL emission for $U_2@I_h(7)$-C_{80} suggests that compared to lanthanide EMFs, the transitions based on the endohedral actinide ions seem to be exceptionally strong and the expected self-absorption effect from the fullerene cage observed for most of the fullerenes studied so far is unable to quench the U or Th based PL emission. It

DOI: 10.1021/jacs.7b10865
J. Am. Chem. Soc. XXXX, XXX, XXX−XXX

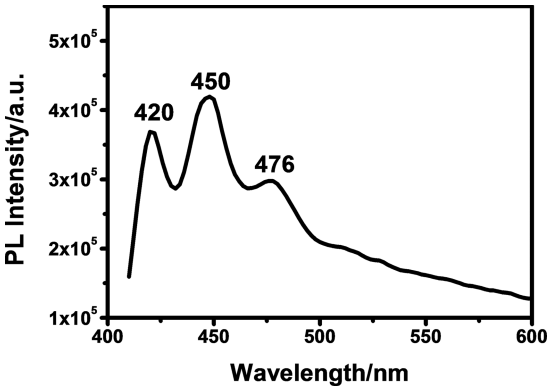

Figure 5. PL spectrum of $U_2@I_h(7)$-C_{80} in CS_2 solution, upon excitation at 406 nm at 298 K.

shows that the charge transfer based photoluminescence is much brighter for actinide EMFs. Thus, the interaction between the actinide ions and the fullerene cages is likely to be substantially different from those for the lanthanide EMFs.

The features of the low-energy Raman spectrum of $U_2@I_h(7)$-C_{80} (Figure 6) show similarities to those of $La_2@I_h$-C_{80} as

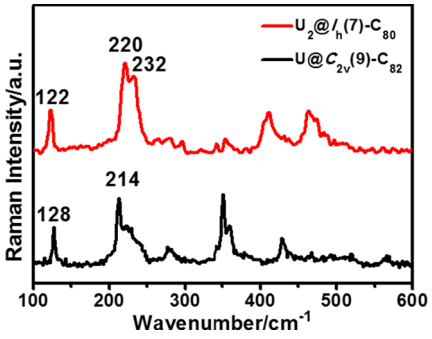

Figure 6. Low-energy Raman spectra of $U_2@I_h(7)$-C_{80} and $U@C_{2v}(9)$-C_{82} in 633 nm excitation.

well as to those of other cluster-fullerenes with I_h-C_{80} cages.[8] One major peak is observed at 122 cm^{-1}. This metal-to-cage vibration has similar but slightly lower wavenumber as compared to that of the $U@C_{2v}(9)$-C_{82}, as shown in Figure 6. In addition, in the range of 200−250 cm^{-1}, major peaks at 220 and 232 cm^{-1} were also observed. The peaks could be assigned to a cage vibrational mode (*Hg*) which is typical for $I_h(7)$-C_{80} based EMFs and agrees well with the crystallographic data.

The redox properties of $U_2@I_h(7)$-C_{80} were investigated by means of cyclic voltammetry (CV) (Figure 7). $I_h(7)$-C_{80} based dimetallic lanthanide EMFs (i.e., $La_2@I_h(7)$-C_{80} and $Ce_2@I_h(7)$-C_{80}) often show almost identical redox potentials, as shown in Table 2. This suggests that due to the very similar nature of the lanthanide ions in lanthanide EMFs, the different encapsulated metal ions will not have a major impact on their redox properties. The redox properties of $U_2@I_h(7)$-C_{80} are very different from those of $La_2@I_h(7)$-C_{80} and $Ce_2@I_h(7)$-C_{80}. The first reduction and oxidation potentials of $U_2@I_h(7)$-C_{80} notably shift ca. 0.15 V negatively compared to those of $La_2@I_h(7)$-C_{80} and $Ce_2@I_h(7)$-C_{80}. The other redox processes also show major differences, as shown in Table 2. These differences indicate that the encapsulation of two U atoms has a major impact on the HOMO and LUMO orbital energies of the

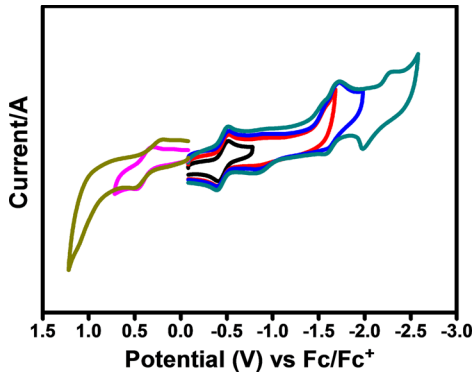

Figure 7. Cyclic voltammogram of $U_2@I_h(7)$-C_{80} in *o*-dichlorobenzene (0.05 M $(n\text{-Bu})_4NPF_6$; scan rate 100 mV/s for CV).

molecule, while a much lower influence is observed for the lanthanide EMFs. Interestingly, despite all these differences, the electrochemical gap for $U_2@I_h(7)$-C_{80}, 0.84 eV, is still very close to those of $La_2@I_h(7)$-C_{80} and $Ce_2@I_h(7)$-C_{80}.

In the 17−18 keV X-ray region, U-$2p_{3/2}$ core electrons can be excited into unoccupied valence orbitals with a U-6d-7s admixture. The XAS spectra for $U_2@I_h(7)$-C_{80} and $U@C_{2v}(9)$-C_{82}, along with those for the reference compounds, uranium sulfate (U^{3+}), uranium oxalate (U^{4+}), and uranium nitrate (U^{6+}) at U L_3-edge are shown in Figure 8. The white line peak of $U_2@I_h(7)$-C_{80} shows an energy very close to that of U^{3+}, as well as to that of the $U@C_{2v}(9)$-C_{82}, which contains a U^{3+} ion inside the fullerene cage.[26] This suggests that $U_2@I_h(7)$-C_{80} has a formal charge state described by $(U^{3+})_2@(C_{80})^{6-}$, which is in perfect agreement with our structural assignment and further confirms the theoretical predictions.[24]

To obtain a better understanding of the experimental results we have made use of computational methods based on density functional theory (see Experimental Details). We have first studied the different possible positions of the two U atoms inside the $I_h(7)$-C_{80} cage according to the occupancies found by the XRD analysis, in particular, those derived from the U(1) and U(2) positions, S_i−S_{iv} models (see Figure 9). The optimized structures are essentially the same as the experimental ones, showing only small deviations of the positions of the U atoms. We have computed the highest spin state of the molecule (septet), considering within the ionic model that (i) electrons in the carbon cage are paired and (ii) there are two U^{3+} (f^3) ions coupled ferromagnetically. The septet was shown to be the lowest energy spin state for $U_2@I_h(7)$-C_{80} and for other diuranium EMFs.[24] The relative energies between these four structures are very similar, within only 1.6 kcal mol^{-1} (see Figure 9 and Table S6), in good agreement with the disorder shown by the U atoms in the crystallographic structure.

The structures with the lowest energies are S_{iii} and S_{iv}, which are symmetry-equivalent, along with S_i. The computed U−U distances for S_{iii} and S_{iv}, 3.74 Å, and for S_i, 3.79 Å (see Table S6), are somewhat longer than the experimental one (3.72 Å) but smaller than those computed previously for the same system.[24] Interestingly, the S_{ii} structure, with the U_2 unit slightly displaced from the C_2 symmetry axis of $I_h(7)$-C_{80}, shows a more compressed U−U distance (3.72 Å), which matches the experimental one. The U−C distances are also rather well-reproduced. For the four structures, the computed spin densities on the U ions are around 3.2 electrons each, in

DOI: 10.1021/jacs.7b10865
J. Am. Chem. Soc. XXXX, XXX, XXX−XXX

Table 2. Redox Potentials (V vs Fc/Fc$^+$) of the $U_2@C_{80}$ and $M_2@I_h$-C_{80} Dimetallofullerenes (M = La and Ce)[a,b]

compound	$E^{2+/+}$	$E^{+/0}$	$E^{0/-}$	$E^{-/2-}$	$E^{2-/3-}$	$E^{3-/4-}$	$E_{gap,ec}$ (V)	ref
$U_2@C_{80}$-I_h[e]	+1.16[c]	+0.40[d]	−0.44[d]	−1.58[c]	−1.78[c]	−2.28[c]	0.84	this work
	[1.15]	[0.40]	[−0.45]	[−1.47]			[0.85]	computations
$La_2@C_{80}$-I_h	+0.95[d]	+0.56[d]	−0.31[d]	−1.71[d]	−2.13[c]		0.87	34
$Ce_2@C_{80}$-I_h	+0.95[d]	+0.57[d]	−0.39[d]	−1.71[d]			0.96	35

[a]Computed oxidation and reduction potentials and electrochemical gaps (in V) along with the experimental values obtained by CV. [b]The computed values are anodically shifted by 150 mV. [c]Peak potential (irreversible redox process). [d]Half-wave potential (reversible redox process). [e]Computed values in square brackets.

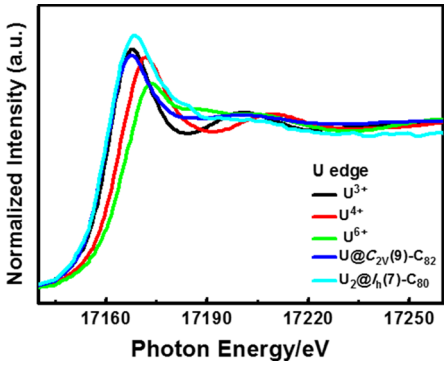

Figure 8. U L_3-edge XAS spectra of of $U_2@I_h(7)$-C_{80}, compared to those of $U@C_{2v}(9)$-C_{82} (blue), NaU^{3+}-sulfate (black), U^{4+}-oxo-hydroxo-formate (red) and uranyl(U^{6+})-nitrate (green).

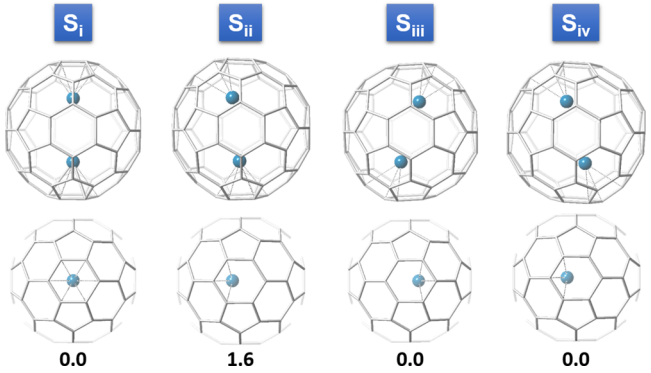

Figure 9. Representations of the optimized structures (S_i–S_{iv}) of $U_2@I_h(7)$-C_{80} and their relative energies in kcal mol^{-1}. Second row, a view from the top, shows the position of the U with respect to the nearest hexagon of the cage. Structures S_{iii} and S_{iv} would be symmetry-equivalent.

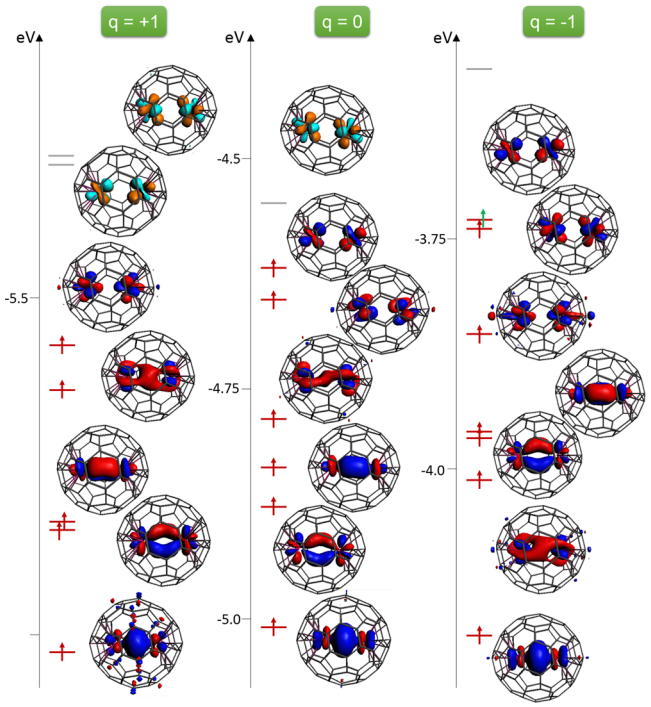

Figure 10. Representation of the occupied and virtual molecular alpha orbitals and their energies for oxidized, neutral and reduced systems $U_2@I_h(7)$-C_{80}^q (q = +1, 0, −1).

line with the f^3 configuration. Foroutan-Nejad et al. recently performed an exhaustive analysis of the bonding in $U_2@I_h(7)$-C_{80} at the BP86/SVP/SDD level and found a double ferromagnetic one-electron two-center U−U bond at a distance of 3.9 Å.[24] In contrast, we found at BP86/TZP level a U−U distance that is slightly shorter (3.74 Å). This distance is much longer than the U−U bond distance of 2.43 Å predicted theoretically for the U_2 molecule.[3] Despite the long distance between uranium ions in the EMF, the topology of the involved orbitals is similar to those reported by Gagliardi and Roos for U_2, even though the overlap between orbitals is lower inside the fullerene. Three of the six occupied orbitals (Figure 10) have a clear U−U bonding nature, whereas for the other three the overlap between the f orbitals is much lower. The U−U interaction was also analyzed using Baders's quantum theory of atoms in molecules (QTAIM).[36] This theory uses different descriptors to analyze bonds via the topology of the electron density. Bader postulated that the presence of a bond critical point (bcp) between two atoms is a necessary and sufficient criterion for the atoms to be bonded. More recently, it has been shown that the delocalization index δ(A, B) provides a quantitative measure of the degree of electron sharing between two atoms. For the U−U interaction, we located a bond critical point in the middle of the two U ions and found a δ(U, U) equal to 0.80, which is larger than the corresponding value (0.37) reported for the La−La bond in $La_2@C_{80}^-$.[14] In this dimetallofullerene, the La−La bond of 3.764 Å is mainly formed via the overlap between s and d orbitals. In addition, we obtained a Mayer bond order for the U−U interaction of 0.34 (Table 3). All these descriptors clearly suggest the presence of a U−U bonding interaction. In order to confirm the existence of this interaction, we have also performed CASSCF calculations for $U_2@I_h(7)$-C_{80} at the computed DFT geometry (see Computational Methods). The ground state was found to be a singlet with an effective bond order of 0.1.[37] Because CASSCF calculations do not include dynamic electron correlation, electrons tend to be overlocalized; thus, the presence of a still perceptible interaction is clearly indicative of U−U coupling. In contrast, the same type of calculations performed on the U_2^{6+} unit at the same metal−metal separation

DOI: 10.1021/jacs.7b10865
J. Am. Chem. Soc. XXXX, XXX, XXX−XXX

Table 3. Spin Multiplicities of the Computed States, U−U Distances, Spin Densities and Selected Bonding Parameters for $U_2@I_h(7)$-$C_{80}{}^q$ (q = +1, 0, and −1)

	q = +1	q = 0	q = −1
2S+1	6	7	8
d_{U-U}[a]	3.820	3.744	3.690
spin	2.90	3.17	3.49
δ(U, U)[b]	0.79	0.80	1.11
BO[c]	0.34	0.34	0.48
ρ(bcp)[d]	0.052	0.090	0.143

[a]Distances in Å. [b]Delocalization index. [c]Mayer bond order. [d]Electron density at bond critical point (in e Å^{-3}).

gives a strongly localized atomic wave function without a bcp point linking the two uranium ions. This fact suggests that the formation of the bcp at the CASSCF level in the EMF arises from the diuranium confinement inside the carbon cage, with an incomplete six electron transfer between guest and host and determined also by the uranium-cage bond formation. As already pointed out, repulsion energies between metal ions in endohedral dimetallofullerenes are much larger than the bonding interactions. Thus, such bonds would immediately dissociate in the absence of the rigid environment provided by the fullerene.[14]

To account for the high disorder found for the U_2 unit inside the $I_h(7)$-C_{80} cage, we have also made other computational models, namely, S_v−S_{ix} (see the Supporting Information), from U positions with lower occupation factors (i.e., U(3)−U(4) (S_v), U(5)−U(6) (S_{vi} and S_{vii}), U(7)−U(8) (S_{viii}), and U(9)−U(10) (S_{ix})). Even though in some of these models the U−U distances are rather short (as for example 3.10 Å in S_{vi}; Table S7), once they have had their geometries optimized the U−U distances for all of them range between 3.62 and 3.79 Å, with final structures very similar to those in S_i−S_{iv} and relative energies ranging between 0 and 5 kcal mol^{-1} (see Table S7). Therefore, computations predict that crystallographic U−U distances below 3.4 Å are very unlikely. The optimized structures from the S_v−S_{ix} models also show bcp's in the middle of the two U atoms and bonding parameters that are similar to those of S_i−S_{iv} (see Table S7).

We have also studied computationally the redox processes observed for $U_2@I_h(7)$-C_{80}. If an arbitrary shift of 150 mV is added to the computed potentials, then the values are in very good agreement with experiment (see Table 2). This means that our computational settings, which are found to provide rather accurate redox potentials for other EMFs,[38,39] are also now working in an acceptable manner, albeit destabilizing the molecular orbitals composed exclusively by U atomic f orbitals by around 0.15 eV. Oxidation and reduction processes take place on U ions (see Figure 10). Therefore, the EC_{gap} is significantly smaller than those predicted for nitride cluster fullerenes $M_3N@I_h(7)$-C_{80} and similar to those of other $M_2@I_h(7)$-C_{80}, which is in line with the experimental results (see Table 2). Interestingly, reduction of the system leads to a decrease of the U−U distance (3.690 Å) and, therefore, to a slight enhancement of this unusual U−U bond. The delocalization index, the Mayer bond order, and the density of the bcp for the U−U bond increase when compared to the values for the neutral molecule (Table 3). Beside, plots of the electron localization function (ELF) on a plane containing the U_2 unit confirm the enhancement of the strength of the U−U bond upon reduction (see Figure S6). In contrast, an increase of the U−U distance and, therefore, a weakening of the U−U bond is observed upon oxidation, even though some of the bond indicators do not appreciably change when compared to the neutral state (see Table 3 and Figure S6). Because the involved uranium orbitals in the redox processes have a low bonding nature (Figure 10), the changes in the U−U bond distances can be also attributed to a change in the formal oxidation state from +3 to +2.5 upon reduction and to +3.5 upon oxidation, which in turn decreases (or increases) the metal−metal repulsion. Thus, the electron accumulation (or depletion) in the intermetal region, and decrease (or increase) of the metal−metal repulsion are interconnected. Foroutan-Nejad et al. already pointed out that the formation of the weak U−U bond inside a fullerene is a consequence of the confinement and not due to the strong orbital overlaps among f orbitals.[24]

Finally, we assigned the peaks observed in the low-energy Raman spectrum of $U_2@I_h(7)$-C_{80}, focusing mainly on the region between 100 and 250 cm^{-1}. Our computations are able to reproduce the most important features of the experimental spectrum in that range. Structures S_i and S_{iii} show a low-frequency peak at around 120 cm^{-1}, corresponding to the longitudinal metal-to-cage mode of the U_2 unit inside the $I_h(7)$-C_{80} cage coupled with the symmetric U−U stretching (see Figure S7). No peak appears for the metal-to-cage vibration based on the longitudinal motion of the U_2 unit as if it were a rigid unit (i.e., with almost no change in the U−U distance; see the Supporting Information). The peaks at 207 and 211 cm^{-1} can be assigned to breathing modes of the cage with no involvement of the U ions. All these peaks appear to be shifted by around 10−20 cm^{-1} to lower frequencies when compared to those obtained experimentally (see Figure 6).

3. CONCLUSIONS

In this work, we report the synthesis and the isolation of a dimetallic actinide EMF, $U_2@C_{80}$. $U_2@C_{80}$ has been fully characterized by mass spectrometry, single crystal X-ray crystallography, UV−vis−NIR, cyclic voltammetry, Raman spectroscopy, PL spectroscopy and XAS. Crystallographic analysis unambiguously assigned the molecular structure to $U_2@I_h(7)$-C_{80} and revealed that the U−U bond distance ranges between 3.46 and 3.79 Å, which is shorter than the 3.9 Å previously predicted for an elongated weak U−U bond inside the C_{80} cage. The XAS results further confirmed that the formal charge state of U inside the fullerene cage is +3, which agrees with previous computational studies and with our crystallographic assignment of an $(I_h$-$C_{80})^{6-}$ cage. Theoretical studies suggest that the different structures derived from the U occupancies obtained from the X-ray structure show low relative energies, in good agreement with the disorder of U atoms observed crystallographically. Furthermore, the theoretical studies confirm the presence of a U−U bonding interaction and find that the singular U−U bond in $U_2@I_h(7)$-C_{80} was slightly strengthened upon reduction and weakened upon oxidation, essentially due to the decrease (increase) in the U−U repulsion when reducing (oxidizing) the system. The comprehensive characterization of $U_2@I_h(7)$-C_{80} and the overall agreement between the experimental data and theoretical investigations provide experimental evidence and deeper understanding of actinide−actinide interactions inside a fullerene cage.

DOI: 10.1021/jacs.7b10865
J. Am. Chem. Soc. XXXX, XXX, XXX−XXX

EXPERIMENTAL DETAILS

Synthesis and Isolation of $U_2@I_h(7)$-C_{80}. The carbon soot containing uranium EMFs were synthesized by the direct-current arc discharge method. The graphite rods, packed with U_3O_8 powders and graphite powders (1:24 molar ratio), were vaporized in the arcing chamber under 200 Torr He atmosphere. The resulting soot was refluxed in chlorobenzene under an argon atmosphere for 12 h. The separation and purification of $U_2@I_h(7)$-C_{80} was achieved by a multistage HPLC procedure. Multiple HPLC columns, including Buckyprep M column (25 × 250 mm, Cosmosil, Nacalai Tesque Inc.), Buckprep-D column (10 × 250 mm, Cosmosil, Nacalai Tesque, Japan), and Buckprep column (10 × 250 mm, Cosmosil, Nacalai Tesque, Japan), were utilized in this procedure. Further details are described in the Supporting Information.

Spectroscopic and Electrochemical Studies. The positive-ion mode matrix-assisted laser desorption/ionization time-of-flight (Bruker, German) was employed for the mass characterization. The UV−vis−NIR spectrum of the purified $U_2@I_h(7)$-C_{80} was measured in CS_2 solution with a Cary 5000 UV−vis−NIR spectrophotometer (Agilent, USA). The Raman spectrum was obtained using a Horiba Lab RAM HR Evolution Raman spectrometer using a laser at 633 nm. Steady-state photoluminescence (PL) spectra were recorded using an FLS980 (Edinburgh Instrument, UK) with excitation at 406 nm at room temperature.

Cyclic voltammetry (CV) and differential pulse voltammetry (DPV) results were obtained in *o*-dichlorobenzene using a CHI-660E instrument. A conventional three-electrode cell consisting of a platinum counter-electrode, a glassy carbon working electrode, and a silver reference electrode was used for both measurements. $(n\text{-}Bu)_4NPF_6$ (0.05 M) was used as supporting electrolyte. The CV and DPV were measured at the scan rate of 100 mV/s and 20 mV/s, respectively.

X-ray absorption spectroscopy (XAS) experiments were performed at the Beijing Synchrotron Radiation Facility (BSRF, beamline 1W1B).

X-ray Crystallographic Study. The black block crystals of $U_2@I_h$-C_{80}·[Ni^{II} (OEP)] were obtained by slow diffusion of a benzene solution of $U_2@I_h$-C_{80} into a $CHCl_3$ solution of [Ni^{II} (OEP)]. X-ray data were collected at 173 K using a diffractometer (APEX II; Bruker Analytik GmbH) equipped with a CCD detector. The multiscan method was used for absorption correction. The structure was solved using direct methods (SIR2004)[40] and refined on F^2 using full-matrix least-squares using SHELXL2014[41] within the WinGX package.[42] Hydrogen atoms were inserted at calculated positions and constrained with isotropic thermal parameters.

Crystal data for $U_2@I_h$-C_{80}·[Ni^{II}(OEP)]·$CHCl_3$: M_r = 2223.27, 0.22 mm × 0.15 mm × 0.11 mm, monoclinic, $C2/m$ (No. 12), a = 25.1208(9) Å, b = 15.5044(6) Å, c = 19.5147(6) Å, α = 90°, β = 95.492(2)°, γ = 90°, V = 7865.8 (5) Å^3, Z = 4, ρ_{calcd} = 1.952 g cm^{-3}, μ(Cu Kα) = 14.136 mm^{-1}, θ = 3.354−74.641, T = 173(2) K, R_1 = 0.1253, wR_2 = 0.3706 for all data; R_1 = 0.1136, wR_2 = 0.3419 for 8027 reflections ($I > 2.0\sigma(I)$) with 1032 parameters. Goodness-of-fit indicator 1.576. Maximum residual electron density 1.653 e Å^{-3}.

Computational Methods. Optimisations without symmetry restrictions of $U_2@I_h(7)$-C_{80} S_i−S_{iv} isomers were carried out with the ADF 2017 package using density functional theory (DFT).[43] The exchange-correlation functionals of Becke and Perdew (BP86) were used. Slater triple-ζ polarization (TZP) basis sets were used to describe the valence electrons of U and C.[44,45] Frozen cores were described by means of single Slater functions, consisting of the 1s shell for C and the 1s to 5d shells for U. Scalar relativistic corrections were included by means of the ZORA formalism. Dispersion corrections by Grimme were also included.[46] Electrochemistry calculations were performed at the same level of theory BP86/TZP, with dichlorobenzene as solvent (COSMO).

Raman spectra were computed using the Gaussian 09 package,[47] since ADF 2017 does not allow Raman intensity calculations for spin unrestricted systems. These calculations were also performed at the DFT level using the BP86 exchange-correlation functional. A double-ζ 6-31G(d,p) basis set was used for carbon atoms and Stuttgart−Dresden basis sets with effective core potential (SDD) for uranium atoms.[48] Optimisation followed by frequency and Raman intensity calculation were computed for the S_i−S_{iii} isomers.

Plots of the electron localization function (ELF) and delocalization indexes of the neutral, reduced and oxidized species of $U_2@I_h(7)$-C_{80} S_{iii} were obtained using the Multiwfn program.[49] Wave functions used for the analysis were obtained by Gaussian 09 single point calculations of the optimized structures obtained with ADF 2017.

CASSCF calculations were performed with Molcas 8.[50] The active space contains 6 electrons distributed in all possible ways over 6 uranium orbitals. Test calculations with larger active spaces do not alter the results; tiny bonding contributions were observed from the U-7s orbitals. The one-electron basis set for uranium has been taken from the study of the neutral U-dimer by Gagliardi and Roos[3] and contains (11s, 10p, 8d, 6f, 3g, 1h) ANO-RCC functions. The same basis set type was used for carbon with (3s, 2p, 1d) functions for each atom of the C_{80} cage. Scalar relativistic effects were included through the Douglas-Kroll-Hess Hamiltonian.

A data set collection of computational results is available in the ioChem-BD repository and can be accessed via https://doi.org/10.19061/iochem-bd-2-20.[51]

ASSOCIATED CONTENT

Supporting Information

The Supporting Information is available free of charge on the ACS Publications website at DOI: 10.1021/jacs.7b10865.

HPLC profiles for the separation of $U_2@I_h$-C_{80} and computational details (PDF)

Additional crystal data for $U_2@I_h$-C_{80}·[Ni^{II}(OEP)]·$CHCl_3$ (CIF)

AUTHOR INFORMATION

Corresponding Authors

*E-mail: josepmaria.poblet@urv.cat.
*E-mail: echegoyen@utep.edu.
*E-mail: fenglai@suda.edu.cn.
*E-mail: chenning@suda.edu.cn.

ORCID

Jun Zhong: 0000-0002-8768-1843
Coen de Graaf: 0000-0001-8114-6658
Antonio Rodríguez-Fortea: 0000-0001-5884-5629
Josep M. Poblet: 0000-0002-4533-0623
Luis Echegoyen: 0000-0003-1107-9423
Lai Feng: 0000-0003-0278-5502
Ning Chen: 0000-0002-9405-6229

Notes

The authors declare no competing financial interest.

ACKNOWLEDGMENTS

We thank all the reviewers for the critical suggestions and substantial input. We cordially thank Prof. Shuao Wang (School of Radiological and Interdisciplinary Sciences, Soochow University) for kind technical support and discussion. This work is supported in part by the NSFC (51772196, 51772195), the NSF of Jiangsu Province (BK20171211), Priority Academic Program Development of Jiangsu Higher Education Institutions (PAPD), and the project of scientific and technologic infrastructure of Suzhou (SZS201708). J.M.P. thanks the Spanish Ministry of Science (CTQ2017-87269-P) and the Generalitat de Catalunya (2013SGR199 and XRQTC) for support and ICREA foundation for an ICREA ACADEMIA award. R.M.-M. thanks Spanish Ministry of Science for a Ph.D. fellowship. L.E. thanks the U.S. National Science Foundation

DOI: 10.1021/jacs.7b10865
J. Am. Chem. Soc. XXXX, XXX, XXX−XXX

(NSF) for generous support under the NSF-PREM program (DMR 1205302) and CHE-1408865 and the Robert A. Welch Foundation for an endowed chair (Grant AH-0033).

REFERENCES

(1) Roos, B. O.; Malmqvist, P. A.; Gagliardi, L. *J. Am. Chem. Soc.* **2006**, *128*, 17000−17006.
(2) Wang, C.-Z.; Gibson, J. K.; Lan, J.-H.; Wu, Q.-Y.; Zhao, Y.-L.; Li, J.; Chai, Z.-F.; Shi, W.-Q. *Dalton Trans.* **2015**, *44*, 17045−17053.
(3) Gagliardi, L.; Roos, B. O. *Nature* **2005**, *433*, 848−851.
(4) Wagner, F. R.; Noor, A.; Kempe, R. *Nat. Chem.* **2009**, *1*, 529−536.
(5) Arnold, P. L.; Jones, G. M.; Odoh, S. O.; Schreckenbach, G.; Magnani, N.; Love, J. B. *Nat. Chem.* **2012**, *4*, 221−227.
(6) Souter, P. F.; Kushto, G. P.; Andrews, L.; Neurock, M. *J. Am. Chem. Soc.* **1997**, *119*, 1682−1687.
(7) Yang, S.; Wei, T.; Jin, F. *Chem. Soc. Rev.* **2017**, *46*, 5005.
(8) Popov, A. A.; Yang, S.; Dunsch, L. *Chem. Rev.* **2013**, *113*, 5989−6113.
(9) Akasaka, T.; Lu, X. *Chem. Rec.* **2012**, *12*, 256−269.
(10) Wang, T.; Wang, C. *Acc. Chem. Res.* **2014**, *47*, 450−458.
(11) Liu, F.; Gao, C.-L.; Deng, Q.; Zhu, X.; Kostanyan, A.; Westerström, R.; Wang, S.; Tan, Y.-Z.; Tao, J.; Xie, S.-Y.; Popov, A. A.; Greber, T.; Yang, S. *J. Am. Chem. Soc.* **2016**, *138*, 14764−14771.
(12) Junghans, K.; Schlesier, C.; Kostanyan, A.; Samoylova, N. A.; Deng, Q.; Rosenkranz, M.; Schiemenz, S.; Westerström, R.; Greber, T.; Büchner, B.; Popov, A. A. *Angew. Chem., Int. Ed.* **2015**, *54*, 13411−13415.
(13) Yang, T.; Zhao, X.; Osawa, E. *Chem. - Eur. J.* **2011**, *17*, 10230−10234.
(14) Popov, A. A.; Avdoshenko, S. M.; Pendas, A. M.; Dunsch, L. *Chem. Commun.* **2012**, *48*, 8031−8050.
(15) Zuo, T. M.; Xu, L. S.; Beavers, C. M.; Olmstead, M. M.; Fu, W. J.; Crawford, D.; Balch, A. L.; Dorn, H. C. *J. Am. Chem. Soc.* **2008**, *130*, 12992−12997.
(16) Umemoto, H.; Ohashi, K.; Inoue, T.; Fukui, N.; Sugai, T.; Shinohara, H. *Chem. Commun.* **2010**, *46*, 5653−5655.
(17) Liu, F.; Krylov, D. S.; Spree, L.; Avdoshenko, S. M.; Samoylova, N. A.; Rosenkranz, M.; Kostanyan, A.; Greber, T.; Wolter, A. U. B.; Buchner, B.; Popov, A. A. *Nat. Commun.* **2017**, *8*, 16098.
(18) Yamada, M.; Kurihara, H.; Suzuki, M.; Saito, M.; Slanina, Z.; Uhlik, F.; Aizawa, T.; Kato, T.; Olmstead, M. M.; Balch, A. L.; Maeda, Y.; Nagase, S.; Lu, X.; Akasaka, T. *J. Am. Chem. Soc.* **2015**, *137*, 232−238.
(19) Bao, L.; Chen, M.; Pan, C.; Yamaguchi, T.; Kato, T.; Olmstead, M. M.; Balch, A. L.; Akasaka, T.; Lu, X. *Angew. Chem., Int. Ed.* **2016**, *55*, 4242−4246.
(20) Shen, W.; Bao, L.; Wu, Y.; Pan, C.; Zhao, S.; Fang, H.; Xie, Y.; Jin, P.; Peng, P.; Li, F.-F.; Lu, X. *J. Am. Chem. Soc.* **2017**, *139*, 9979−9984.
(21) Guo, T.; Diener, M. D.; Chai, Y.; Alford, M. J.; Haufler, R. E.; McClure, S. M.; Ohno, T.; Weaver, J. H.; Scuseria, G. E.; Smalley, R. E. *Science* **1992**, *257*, 1661.
(22) Wu, X.; Lu, X. *J. Am. Chem. Soc.* **2007**, *129*, 2171−2177.
(23) Infante, I.; Gagliardi, L.; Scuseria, G. E. *J. Am. Chem. Soc.* **2008**, *130*, 7459−7465.
(24) Foroutan-Nejad, C.; Vicha, J.; Marek, R.; Patzschke, M.; Straka, M. *Phys. Chem. Chem. Phys.* **2015**, *17*, 24182−24192.
(25) Wang, Y.; Morales-Martínez, R.; Zhang, X.; Yang, W.; Wang, Y.; Rodríguez-Fortea, A.; Poblet, J. M.; Feng, L.; Wang, S.; Chen, N. *J. Am. Chem. Soc.* **2017**, *139*, 5110−5116.
(26) Cai, W.; Morales-Martinez, R.; Zhang, X.; Najera, D.; Romero, E. L.; Metta-Magana, A.; Rodriguez-Fortea, A.; Fortier, S.; Chen, N.; Poblet, J. M.; Echegoyen, L. *Chem. Sci.* **2017**, *8*, 5282−5290.
(27) Kratschmer, W.; Lamb, L. D.; Fostiropoulos, K.; Huffman, D. R. *Nature* **1990**, *347*, 354−358.
(28) Feng, L.; Suzuki, M.; Mizorogi, N.; Lu, X.; Yamada, M.; Akasaka, T.; Nagase, S. *Chem. - Eur. J.* **2013**, *19*, 988−993.
(29) Nishibori, E.; Takata, M.; Sakata, M.; Taninaka, A.; Shinohara, H. *Angew. Chem., Int. Ed.* **2001**, *40*, 2998−2999.
(30) Pyykkö, P. *J. Phys. Chem. A* **2015**, *119*, 2326−2337.
(31) Dognon, J.-P.; Clavaguéra, C.; Pyykkö, P. *J. Am. Chem. Soc.* **2009**, *131*, 238−243.
(32) Cooper, O. J.; Mills, D. P.; McMaster, J.; Tuna, F.; McInnes, E. J. L.; Lewis, W.; Blake, A. J.; Liddle, S. T. *Chem. - Eur. J.* **2013**, *19*, 7071−7083.
(33) Zheng, T.; Wu, Q.-Y.; Gao, Y.; Gui, D.; Qiu, S.; Chen, L.; Sheng, D.; Diwu, J.; Shi, W.-Q.; Chai, Z.; Albrecht-Schmitt, T. E.; Wang, S. *Inorg. Chem.* **2015**, *54*, 3864−3874.
(34) Suzuki, T.; Maruyama, Y.; Kato, T.; Kikuchi, K.; Nakao, Y.; Achiba, Y.; Kobayashi, K.; Nagase, S. *Angew. Chem., Int. Ed. Engl.* **1995**, *34*, 1094−1096.
(35) Yamada, M.; Nakahodo, T.; Wakahara, T.; Tsuchiya, T.; Maeda, Y.; Akasaka, T.; Kako, M.; Yoza, K.; Horn, E.; Mizorogi, N.; Kobayashi, K.; Nagase, S. *J. Am. Chem. Soc.* **2005**, *127*, 14570−14571.
(36) Bader, R. F. W. *Atoms in Molecules - A Quantum Theory*; Oxford University Press: Oxford, U.K., 1990.
(37) Roos, B. O.; Borin, A. C.; Gagliardi, L. *Angew. Chem.* **2007**, *119*, 1491−1494.
(38) Valencia, R.; Rodríguez-Fortea, A.; Clotet, A.; de Graaf, C.; Chaur, M. N.; Echegoyen, L.; Poblet, J. M. *Chem. - Eur. J.* **2009**, *15*, 10997−11009.
(39) Abella, L.; Wang, Y.; Rodríguez-Fortea, A.; Chen, N.; Poblet, J. M. *Inorg. Chim. Acta* **2017**, *468*, 91.
(40) Burla, M. C.; Caliandro, R.; Camalli, M.; Carrozzini, B.; Cascarano, G. L.; De Caro, L.; Giacovazzo, C.; Polidori, G.; Spagna, R. *J. Appl. Crystallogr.* **2005**, *38*, 381−388.
(41) Sheldrick, G. *Acta Crystallogr., Sect. C: Struct. Chem.* **2015**, *71*, 3−8.
(42) Farrugia, L. *J. Appl. Crystallogr.* **2012**, *45*, 849−854.
(43) te Velde, G.; Bickelhaupt, F. M.; Baerends, E. J.; Fonseca Guerra, C.; van Gisbergen, S. J. A.; Snijders, J. G.; Ziegler, T. *J. Comput. Chem.* **2001**, *22*, 931−967.
(44) Becke, A. D. *J. Chem. Phys.* **1986**, *84*, 4524−4529.
(45) Perdew, J. P. *Phys. Rev. B: Condens. Matter Mater. Phys.* **1986**, *33*, 8822−8824.
(46) Grimme, S.; Ehrlich, S.; Goerigk, L. *J. Comput. Chem.* **2011**, *32*, 1456−1465.
(47) Frisch, M. J.; Trucks, G. W.; Schlegel, H. B.; Scuseria, G. E.; Robb, M. A.; Cheeseman, J. R.; Scalmani, G.; Barone, V.; Mennucci, B.; Petersson, G. A.; Nakatsuji, H.; Caricato, M.; Li, X.; Hratchian, H. P.; Izmaylov, A. F.; Bloino, J.; Zheng, G.; Sonnenberg, J. L.; Hada, M.; Ehara, M.; Toyota, K.; Fukuda, R.; Hasegawa, J.; Ishida, M.; Nakajima, T.; Honda, Y.; Kitao, O.; Nakai, H.; Vreven, T.; Montgomery, J. A., Jr.; Peralta, J. E.; Ogliaro, F.; Bearpark, M.; Heyd, J. J.; Brothers, E.; Kudin, K. N.; Staroverov, V. N.; Kobayashi, R.; Normand, J.; Raghavachari, K.; Rendell, A.; Burant, J. C.; Iyengar, S. S.; Tomasi, J.; Cossi, M.; Rega, N.; Millam, J. M.; Klene, M.; Knox, J. E.; Cross, J. B.; Bakken, V.; Adamo, C.; Jaramillo, J.; Gomperts, R.; Stratmann, R. E.; Yazyev, O.; Austin, A. J.; Cammi, R.; Pomelli, C.; Ochterski, J. W.; Martin, R. L.; Morokuma, K.; Zakrzewski, V. G.; Voth, G. A.; Salvador, P.; Dannenberg, J. J.; Dapprich, S.; Daniels, A. D.; Farkas, O.; Foresman, J. B.; Ortiz, J. V.; Cioslowski, J.; Fox, D. J. *Gaussian 09*, revision D.01; Gaussian, Inc.: Wallingford, CT, 2009.
(48) Cao, X.; Dolg, M. *J. Mol. Struct.: THEOCHEM* **2002**, *581*, 139−147.
(49) Lu, T.; Chen, F. *J. Comput. Chem.* **2012**, *33*, 580−592.
(50) Aquilante, F.; Autschbach, J.; Carlson, R. K.; Chibotaru, L. F.; Delcey, M. G.; De Vico, L.; Fdez. Galván, I.; Ferré, N.; Frutos, L. M.; Gagliardi, L.; Garavelli, M.; Giussani, A.; Hoyer, C. E.; Li Manni, G.; Lischka, H.; Ma, D.; Malmqvist, P. Å.; Müller, T.; Nenov, A.; Olivucci, M.; Pedersen, T. B.; Peng, D.; Plasser, F.; Pritchard, B.; Reiher, M.; Rivalta, I.; Schapiro, I.; Segarra-Martí, J.; Stenrup, M.; Truhlar, D. G.; Ungur, L.; Valentini, A.; Vancoillie, S.; Veryazov, V.; Vysotskiy, V. P.; Weingart, O.; Zapata, F.; Lindh, R. *J. Comput. Chem.* **2016**, *37*, 506−541.

DOI: 10.1021/jacs.7b10865
J. Am. Chem. Soc. XXXX, XXX, XXX−XXX

(51) Álvarez-Moreno, M.; de Graaf, C.; López, N.; Maseras, F.; Poblet, J. M.; Bo, C. *J. Chem. Inf. Model.* **2015**, *55*, 95−103.

DOI: 10.1021/jacs.7b10865
J. Am. Chem. Soc. XXXX, XXX, XXX−XXX